

X-ray Observations of the Broad-Line Radio Galaxy 3C 390.3

Karen M. Leighly^{1,2}
leighly@postman.riken.go.jp

Paul T. O'Brien³
pto@star.le.ac.uk

Rick Edelson⁴
edelson@spacly.physics.uiowa.edu

Ian M. George^{5,6}
george@heavx.gsfc.nasa.gov

Matthew A. Malkan⁷
malkan@bonnie.astro.ucla.edu

Masaru Matsuoka¹
matsuoka@postman.riken.go.jp

Richard F. Mushotzky⁵
mushotzky@heavx.gsfc.nasa.gov

Bradley M. Peterson⁸
peterson@payne.mps.ohio-state.edu

ABSTRACT

We present the data and preliminary analysis for a series of 90 *ROSAT* HRI and two *ASCA* observations of the broad-line radio galaxy 3C 390.3. These data were obtained during the period 1995 January 2 to 1995 October 6 as part of an intensive multiwavelength monitoring campaign. The soft X-ray flux in the *ROSAT* band varied by nearly a factor of four during the campaign, and the well-resolved light-curve shows several distinct features. Several large amplitude flares were observed, including one in which the flux increased by a factor of about 3 in 12 days. Periods of reduced variability were also seen, including one nearly 30 days long. While the HRI hardness

¹Cosmic Radiation Laboratory, RIKEN, Hirosawa 2-1, Wako-shi, Saitama 351, Japan

²Current address: Columbia Astrophysics Laboratory, 538 West 120th Street, New York, NY 10027

³Department of Physics & Astronomy, University of Leicester, University Road, Leicester, LE1 7RH, U.K.

⁴Department of Physics and Astronomy, University of Iowa, Iowa City, IA 52242-1479

⁵Code 660.2, NASA Goddard Space Flight Center, Greenbelt, MD 20771

⁶Also Universities Space Research Association

⁷Department of Astronomy, University of California, Los Angeles, CA, 90024-1562

⁸Department of Astronomy, Ohio State University, 174 W. 18th Ave., Columbus, OH 43210-1106

ratio decreased significantly, it is apparently consistent with that expected due to the detector during the monitoring period.

The two *ASCA* observations were made on 1995 January 15 and 1995 May 5. The 0.5–10.0 keV spectra can be adequately described by an absorbed power-law. There is no evidence for a soft excess in the *ASCA* spectra, indicating that the *ROSAT* HRI is sampling variability of the X-ray power-law. A broad iron line was observed in a longer 1993 *ASCA* observation, and while there is statistical evidence that the line is present in the 1995 spectra, it could not be resolved clearly. There is evidence, significant at > 90% confidence, that the photon index changed from 1.7 to 1.82 while the flux increased by 63%. The spectral change can be detected in the spectra below 5 keV, indicating that the origin cannot be a change in ratio of reflected to power-law flux. A compilation of results from *ASCA* and *Ginga* observations show that on long time scales the intrinsic photon index is correlated with the flux.

Subject headings: galaxies: individual (3C 390.3) – X-rays: galaxies – galaxies: active

1. Introduction

3C 390.3 is a luminous ($L_{X(2-10)} \sim 2 - 4 \times 10^{44}$ ergs s⁻¹) nearby ($z=0.057$) broad-line radio galaxy located in the North Ecliptic cap. It is well known as the prototypical source of broad double-peaked and variable $H\beta$ lines (Eracleous & Halpern 1994; Veilleux & Zheng 1991). It has a superluminal compact kiloparsec scale radio jet as well as two extended radio lobes, each with a hot spot (e.g. Alef et al. 1996). 3C 390.3 is variable in all wave bands on time scales from days to years, including the optical (Barr et al. 1980) and UV (Clavel & Wamsteker 1987). It is a bright and variable X-ray source, and has been observed many times in X-rays (see Eracleous, Halpern & Livio 1996 for a compilation). Hard X-ray variability by a factor of 2 was reported over a period of 6 weeks when observed with *OSO 7* (Mushotzky, Baity & Peterson 1977). Variability by a factor of 6 was observed among 6 observations made by the EXOSAT observatory (Inda et al. 1994). Historically, the spectrum has generally been well described by an absorbed power-law. Evidence that the measured column density exceeds the Galactic and may be variable has been found in several observations (Eracleous et al. 1996 and references therein). Photon index variability has also been found; between two *Ginga* observations 2.5 years apart, Inda et al. (1994) found a change in photon index from 1.76 to 1.54 when the flux decreased by $\sim 30\%$. Evidence for an iron $K\alpha$ line was also found in the *Ginga* spectra (Inda et al. 1994). The iron line was resolved in a 1993 *ASCA* observation and the measured velocity width of $\sim 16,500$ km/s is consistent with an origin in an accretion disk at about 250 gravitational radii (Eracleous et al. 1996).

During 1995, 3C 390.3 was subject to a monitoring campaign from radio through X-rays. Using the *ROSAT* HRI, we obtained the first well-sampled X-ray light-curve on time scales from days to months. This paper presents the *ROSAT* data as well as two *ASCA* observations obtained

during the monitoring period. The soft X-ray variability is briefly described, but the results of the detailed timing analysis, and the results from the optical, UV and radio monitoring will be reported elsewhere (Leighly & O’Brien 1997, Dietrich et al. 1997, O’Brien et al. 1997, Leighly et al. 1997).

2. *ROSAT* Data

Ninety-three *ROSAT* HRI observations of 3C 390.3 each 1500 seconds with monitoring interval of three days were scheduled. Ninety observations were successful, and only three observations were missed. Excluding these, the mean interval was 3.22 days with standard deviation 0.75 days. The first observation began 2 January 1995 5:05 and the last observation ended 6 October 1995 11:10. The background subtracted light-curve is shown in the upper panel of Figure 1, and the *ROSAT* data sequence numbers, dates of observation, exposures and count rates are given in Table 1. Note that the dates are given for the midpoint of the observation, and no barycentric correction has been applied.

The *ROSAT* HRI is an ideal instrument for monitoring the soft X-ray flux from 0.1–2.0 keV. The instrument is sensitive to low fluxes because the background is low. The FWHM of the main component of the image point spread function is $1.7''$, broadened somewhat by the attitude reconstruction uncertainty of about $6 - 10''$. Thus the source photons can be extracted from a small region, reducing further the statistical error from background subtraction. We used a source extraction region $1.5'$ in radius, and the background was estimated from an annulus with radii $2.5'$ and $5'$. These regions are near the center of the detector where the image is fairly flat, so no off-axis response correction as applied. The background count rate was variable, but because the background rate was only about 5% of the source count rate, it was only necessary to exclude intervals with very large spikes.

3. *ROSAT* Analysis

3.1. Variability

The light-curve in Figure 1 shows that significant, large amplitude soft X-ray variability occurred during the monitoring period. We chose the 3 day monitoring interval based on the fact that only low amplitude variability was detected during single day observations by *ROSAT* and *Ginga*, but measurable variability occurred between observations several days apart. This choice is vindicated by the fact that significant variability was not found during individual *ROSAT* observations (all of which were made within one or two satellite orbits), but variability of up to 50% was found between adjacent observations.

The most noticeable feature in the *ROSAT* light-curve is a flare around TJD 9800 in which

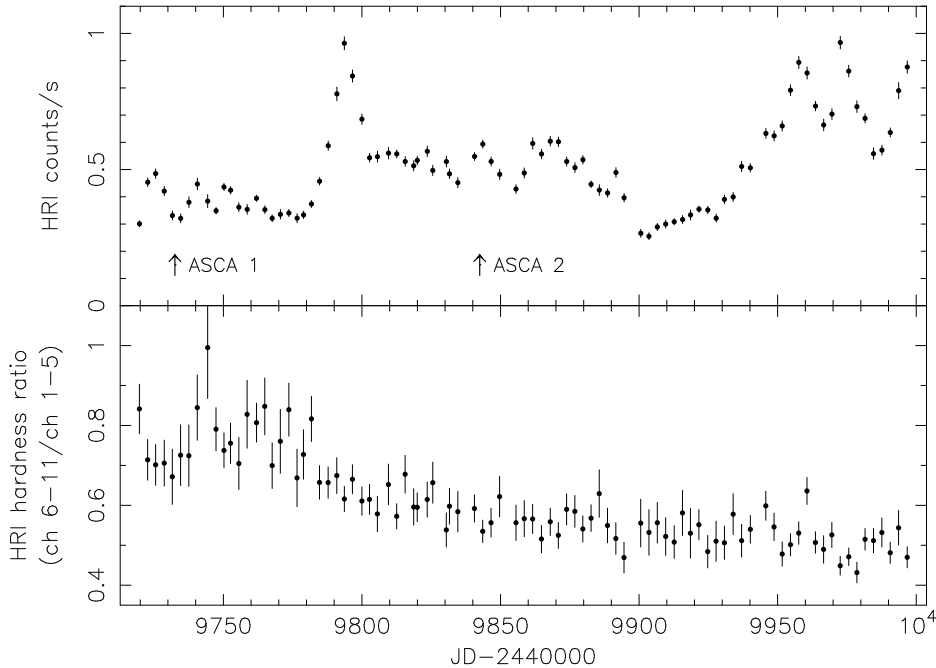


Fig. 1.— Top: *ROSAT* HRI light-curve from monitoring observations of 3C 390.3. The times of the two *ASCA* observations are marked with arrows. Using the distributed HRI response matrix and ignoring the effects of the gain change, 1 count/s corresponds to 2.93 and 3.04×10^{-11} ergs $\text{s}^{-1}\text{cm}^{-2}$ for photon indices 1.7 and 1.82 respectively and $N_H = 1.15 \times 10^{21}$ cm^{-2} . Bottom: The HRI hardness ratio shows that the spectrum becomes steadily steeper as a function of time. However, the steepening likely is dominated by the temporal gain of the detector and cannot be used to study the spectral variability.

the flux increased by a factor of 3 in about 12 days, and then decreased by a factor of 2 in about 9 days. A series of similar flares is apparent after TJD 9950. These contrast markedly with periods of reduced variability, which seem to occur preferentially before and after the flares and most notably during a period of about 30 days starting at about TJD 9900. A discussion and interpretation of this distinctive variability is given in Leighly & O’Brien (1997).

During the *ROSAT* campaign the average source count rate was 0.5 cnt s^{-1} while the average background count rate in the source region was 0.027 cnt s^{-1} , yielding an average uncertainty in the count rate of 0.017 cnt s^{-1} . The average effective exposure was ~ 1900 s and the average signal-to-noise was ~ 30 . The ratio of the largest to smallest flux, R_{max} , is 3.8, demonstrating that a large amplitude of variability was observed in soft X-rays during this campaign. The fractional variability amplitude (F_{var}) is defined as the standard deviation of the flux divided by the mean flux, and gives a measure of the magnitude of the variability during the observation (e.g. Edelson et al. 1996). The true standard deviation is used, i.e. the mean measurement error

has been subtracted in quadrature. For this series of observations, the F_{var} is 0.328. Because the monitoring spanned a comparatively long period of time, the observed amplitude of variability is large compared with previous observing campaigns in X-rays. For example, in the previous AGN Watch monitoring campaign of NGC 4151, the F_{var} from 13 *ROSAT* PSPC and 4 *ASCA* observations in the 1–2 keV band was 23.9%, but note that the monitoring period was just 10 days.

The time scale of variability appears relatively long. In comparison, during an *ASCA* observation of MCG –6-30-15, variability by a factor of 1.5 was observed in 100 seconds (Reynolds et al. 1995). However, it has been found that various measures of the variability time scale are correlated with the luminosity (Lawrence & Papadakis 1993). In the *ASCA* observations reported here (see below), the 2–10 keV luminosity was found to be $2 - 4 \times 10^{44}$ erg s⁻¹. Thus 3C 390.3 is a relatively luminous object compared with many well studied X-ray variable Seyfert 1s including MCG –6-30-15 ($L_X = 1.1 \times 10^{43}$ erg s⁻¹). From the correlation between doubling time scale and luminosity obtained from EXOSAT data by Lawrence & Papadakis (1993), this luminosity should correspond to a doubling time scale of $\sim 10^6$ s, which is approximately 12 days, or the time scale of the flare. Thus the longer observed time scale of variability is consistent with the greater luminosity of this object.

3.2. Spectral Variability

The HRI hardness ratio, defined as the ratio of counts in channels 6–10 to 1–5, varies significantly during the monitoring period (Figure 1). While the spectral response of the *ROSAT* HRI is not well determined, the hardness ratio gives some indication of differences in spectra (David et al. 1996). However, it is known that there is a temporal gain variation in the HRI, such that the photons are detected in progressively lower channels, thus producing smaller values of the hardness ratio (David et al. 1996), as observed. This must be the source of at least part of the hardness ratio change. Two *ASCA* observations during the monitoring period show significant spectral variability in the same sense as the HRI hardness ratio change (see below), but repeated spectral simulations using the HRI response matrix obtained before launch and the *ASCA* best fit models give indistinguishable mean PHA and hardness ratios. While the shift in the mean channel of the 3C 390.3 spectra is larger than the shift observed from four calibration observations of the supernova remnant N132D contemporaneous with the monitoring campaign (J. Pye, J. Silverman 1996 p. comm.), that may be expected because the spectrum of 3C 390.3 is harder. In conclusion, we can make no definite statement about the spectral variability during the monitoring period from the HRI hardness ratio.

4. ASCA Data

Two 20ks *ASCA* observations were made during the *ROSAT* monitoring campaign. These started 1995 January 15 9:17 and 1995 May 5 23:57, and are hereafter referred to as the first and second observations. The angles between the telescope axes (XRT) and the Sun were 101.3 and 79.2 degrees and the observing modes were 2CCD Bright mode and 1CCD Faint mode for the first and second observations, respectively. The times of these observations are marked in the upper panel of Figure 1. Events were excluded when the satellite was in the South Atlantic Anomaly (SAA), and at the beginning of the observation when the attitude was unstable. The following selection criteria were used: coefficient of rigidity $> 6 \text{ GeV}/c$; elevation angle $> 5^\circ$; radiation belt monitor count rate (RBM_CONT) $< 200 \text{ cnts s}^{-1}$. For the SIS detectors, the hot and flickering pixels were removed, and the further selection criteria were used: bright earth angle $> 15^\circ$; events collected within 4 readout cycles (32 and 16 s for the first and second observations, respectively) after passage through the SAA and the day–night terminator were excluded; events collected above the threshold of 400 pixels per CCD per readout were excluded; event grades 0 and 2–4 were used. The standard pulse-height versus rise time filter was applied to GIS events. The source spectra were obtained from regions of radius 4 arcmin and 6 arcmin for the SIS and GIS respectively. The background spectra were obtained from source free regions of the same chip for the SIS, and from regions as close as possible to the same distance from the optical axis as the source region for the GIS. SIS response matrices appropriate for the time of the observation were made. The spectra were fit between 0.5–10.0 keV and 0.8–10.0 keV for the SIS and GIS respectively.

The XRT–sun angle was somewhat low during the second observation, so there was the possibility of contamination by light leakage. We carefully examined the SIS spectra using various constraints on the bright earth elevation angle and found no evidence for light leakage.

While most of the spectra were fit well by an absorbed power-law model, residuals including a hard tail and a soft excess were observed in fits of the SIS1 spectrum from the January observation. In addition, absorption column versus photon index χ^2 contours from the SIS0 and SIS1 spectra were inconsistent at the 90% confidence level. This observation was made in 2CCD Bright mode, which means that while data collected at medium bit rate were compressed on-board, the greater telemetry rate during high bit rate transmission allowed the data to be sent to the ground before compression. The high bit rate data must be compressed before analysis, but because that is done on the ground, additional calibration including correction for echo and dark frame error (DFE) is possible before compression. During this observation, approximately half the data were collected at high bit rate. Thus we collected corrected high bit rate spectra separately and found that the contours generated from these spectra from both detectors were consistent with the uncorrected SIS0 contour, but the uncorrected SIS1 contour was offset. Because of this behavior, the medium bit rate data from SIS1 of the January observation was judged anomalous, although the cause is not known, and the high bit rate spectrum from that detector was used in further spectral fits. The observation log is given in Table 2.

5. ASCA Analysis

The count rates listed in Table 2 indicate that the flux changed significantly between the two observations. The spectra from all four detectors from both observations were fit simultaneously with a power-law plus absorption model, allowing the normalization to be free between the two observations. The resulting fit was acceptable: χ^2 was 2262/2124 degrees of freedom (d.o.f.), the photon index was 1.76 and the absorption column was $1.0 \times 10^{21} \text{ cm}^{-2}$. Allowing the photon index to vary between the two observations gave a better fit with $\chi^2 = 2183/2123$ d.o.f. The change in χ^2 of 79 indicates with $> 99.9\%$ confidence obtained using the F test for one additional degree of freedom that a significant change in photon index occurred between these two observations. Alternatively, allowing only the absorption to vary yields $\chi^2 = 2207/2123$ d.o.f. Allowing both to vary gives $\chi^2 = 2182/2122$ d.o.f., so there is no evidence that both the absorption and the photon index vary. When the absorption was equated between the two observations, the best fit column was $1.1 \times 10^{21} \text{ cm}^{-2}$ and the two best fit indices were 1.68 and 1.80. These photon indices are in the range typical for an AGN, although flatter than the average (e.g. Nandra & Pounds 1994).

There is no evidence for a soft excess component in the residuals of the power-law fit to the ASCA spectra. The HRI response is harder than that of the ROSAT PSPC. There is a little sensitivity to photons in the 0.1–0.4 keV range, but most of the effective area is above 0.4 keV and therefore the band passes of the HRI and ASCA SIS overlap almost completely. This means that the HRI is sampling the variability of the X-ray power-law.

A broad iron $K\alpha$ line was discovered in the previous 1993 observation of 3C 390.3 (Eracleous et al. 1996). The exposures here are shorter, and the presence of the broad line cannot be clearly seen in the residuals (Figure 2). A Gaussian line was added to the model, with the parameters between the two observations constrained to be equal. When the energy is fixed at 6.4 keV in the rest frame and the width is narrow, the fit was improved by $\Delta\chi^2 = -7$, significant with $> 99\%$ confidence evaluated using the F statistic. Allowing either the line energy or the line width to vary results in further improvement in fit by $\Delta\chi^2 = -10$ which is significant at $> 99.5\%$ confidence. In this case, the line energy shifts to a lower value, and the line width increases (Table 3), as expected if the line is emitted from a rotating disk (e.g. Matt et al. 1992). Finally, allowing the remaining parameter to vary does not result in a significant improvement in fit ($\Delta\chi^2 = 1$). This suggests that the broad line is certainly present in the spectra, but the shorter exposures don't allow us to clearly resolve it. No reduction of χ^2 results when the line normalization is allowed to vary between the two observations. The parameters from the best fit spectra are listed in Table 3. The measured line parameters are consistent with those obtained by Eracleous et al. (1996). The physical width of the line was frozen at the best fit value to avoid fitting instability during error analysis. The quoted uncertainties are 90% for two parameters of interest ($\Delta\chi^2 = 4.61$). Figure 3 shows the photon index vs $N_H \chi^2$ contours for the two observations (solid line). These indicate that the photon index varied at $> 90\%$ significance between the two observations, while the absorption remained the same.

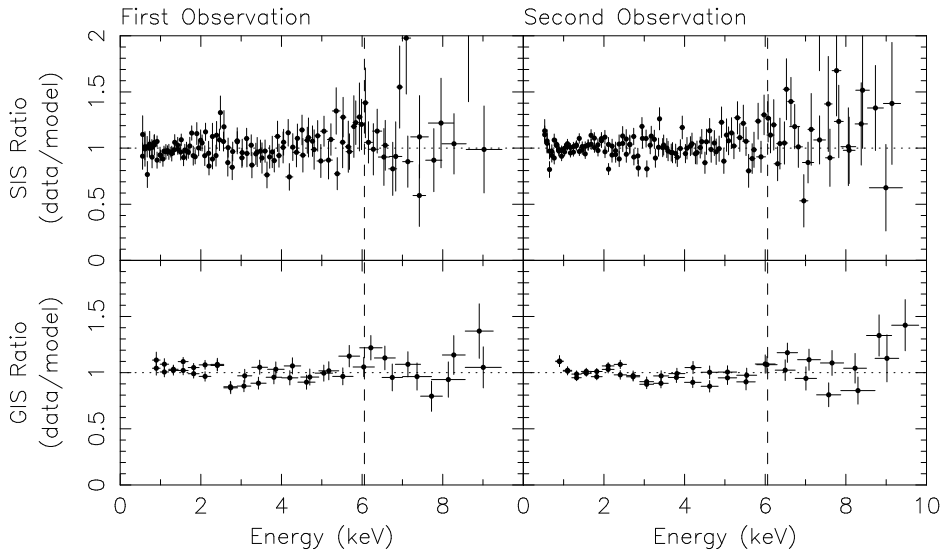


Fig. 2.— The ratio of data to an absorbed power-law model for the two *ASCA* observations. The vertical dotted line marks the location of the cosmologically redshifted iron $K\alpha$ line. While addition of a broad iron line to the model significantly improves the spectral fit, these residuals show that the evidence for the iron line in these data is not very strong, probably because the observations were shorter than the 1993 observation discussed by Eracleous, Halpern & Livio (1993). Also, no evidence for a soft excess component is seen.

The photon index and flux measured in the first 1995 *ASCA* observation were consistent with those measured during the 1993 observation (Eracleous et al. 1996). The column density is larger but only at the 68% confidence level than that measured by Eracleous et al. (1996), suggesting support for their idea that the absorption intrinsic to the source changes slowly over time. It also confirms their observation that the absorption is significantly larger than the Galactic column in that direction of $3.7 \times 10^{20} \text{ cm}^{-2}$ (Murphy et al. 1996). Analysis of a 20ks archival *ROSAT* PSPC observation also shows absorption in excess of Galactic at $\sim 6 \times 10^{20} \text{ cm}^{-2}$.

The recent reanalysis done by Wozniak et al. (1996) shows that there is evidence for a weak reflection component (e.g. Nandra & Pounds 1994) in the *Ginga* spectra from 3C 390.3. In the presence of a reflection component, spectral variability could be observed if the relative normalization between the power-law and reflection varied. Physically, this could occur if the reflection region is extended or very far from the nucleus, so that the change of reflected flux is lagged or smeared compared with the input flux (e.g. Leighly et al. 1996). In this case, the spectrum would be expected to steepen as the flux increases, as observed. However, in the standard case, i.e. if the isotropic X-ray source is illuminating cold material subtending 2π steradians, the reflection component cannot be detected below about 5 keV (e.g. Weaver et al. 1995). To test the effect of reflection on the spectral variability, we fit the spectra simultaneously

for energies below 5 keV. In Figure 3 the photon index vs $N_H \chi^2$ contours for this fit are shown (dashed line). These indicate that the spectral variability can still be detected in this band, demonstrating that it cannot be attributed to a change in the relative normalization between the reflection and power-law components.

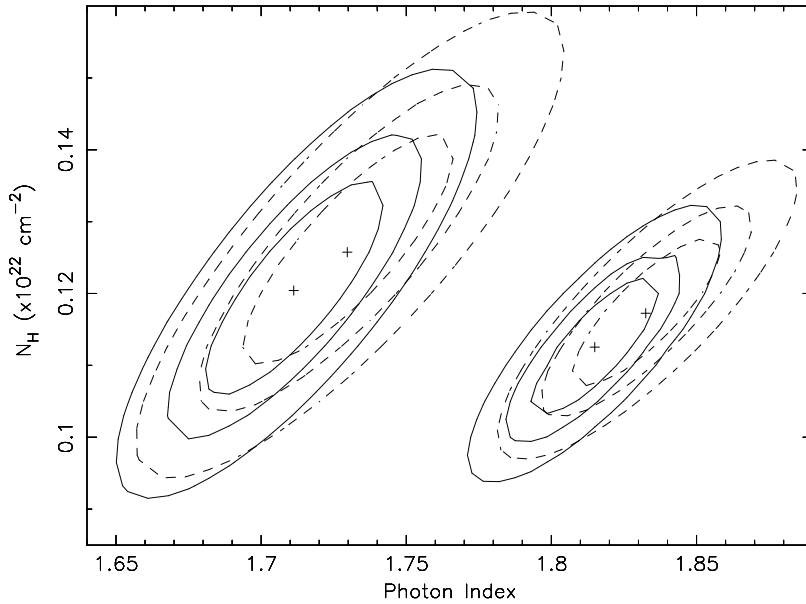


Fig. 3.— Photon index versus $N_H \chi^2$ contours (99%, 90% and 68%) for the two *ASCA* observations. These demonstrate that the photon index differs significantly between these two observations. The solid line shows the results from fitting over the full 0.5–10.0 keV range, while the dashed line shows the results from the restricted range 0.5–5 keV. The results are consistent for the two ranges, demonstrating that the spectral variability cannot be attributed to a change in the relative normalization of the power-law and reflection components.

5.1. The Spectral Variability

The photon index change in the *ASCA* data, with an increase in flux, implies a pivot point for the spectrum of ~ 400 keV for 3C 390.3. Zdziarski et al. (1995) discuss the average X-ray and γ -ray spectra from *Ginga* and *CGRO* OSSE from groups partitioned according to their optical and radio characteristics. The mean spectrum from the radio-loud group, consisting of 3C 390.3 and 3C 311, when fit with a thermal Comptonization model, gave a thermal cutoff of $E_C = 480_{-190}^{+670}$ keV. While not well constrained, this value is consistent with the pivot point of the spectral variability.

Photon index variability has been previously observed in the *Ginga* spectra from 3C 390.3 (Inda et al. 1991; Wozniak et al. 1996). Table 4 gives a compilation of the photon indices and

fluxes from the Ginga and *ASCA* observations. We don't consider observations from previous observatories including EXOSAT because the parameters are much more poorly constrained for this fairly faint source (Inda et al. 1991). Because we are interested in the intrinsic photon index, we use values from fits which include the reflection model taken from Wozniak et al. (1997) and Eracleous et al. (1996). For the *ASCA* observations reported in this paper, we use the values obtained from fits below 5 keV. The flux plotted against the photon index is shown in Figure 4.

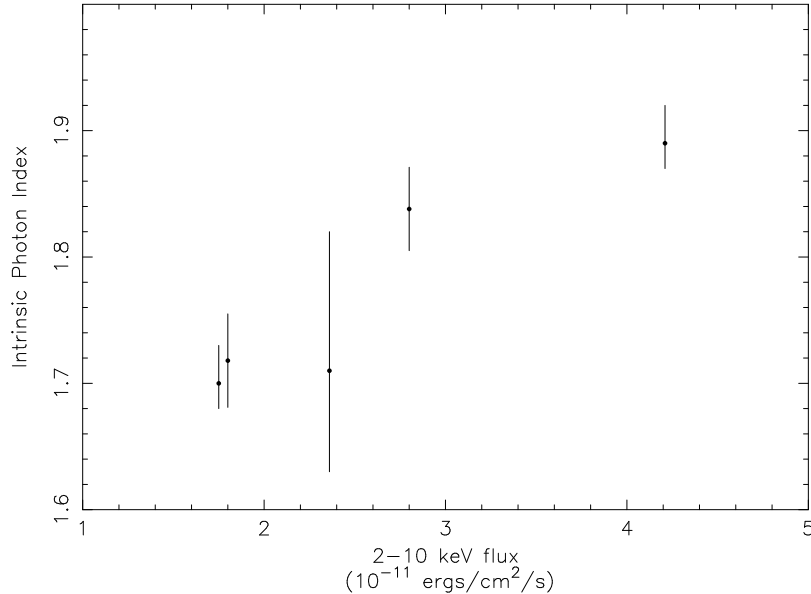


Fig. 4.— Photon index versus $N_H \chi^2$ contours (99%, 90% and 68%) for the two *ASCA* observations. These demonstrate that the photon index differs significantly between these two observations. The solid line shows the results from fitting over the full 0.5–10.0 keV range, while the dashed line shows the results from the restricted range 0.5–5 keV. The results are consistent for the two ranges, demonstrating that the spectral variability cannot be attributed to a change in the relative normalization of the power-law and reflection components.

The photon index changes from roughly 1.7 to 1.9 as the flux doubles, and a general correlation of the flux and photon index is seen. This is similar to that observed from NGC 4151 (Yaqoob & Warwick 1991) and NGC 5548 (Nandra et al. 1993). Recently, Haardt, Maraschi & Ghisellini (1997) investigated spectral variability in the context of thermal disk-corona models. The change in photon index measured here for the factor of two change in flux is too large to be explained by the simplest pair-dominated reprocessing models. Rather, it suggests that scattering optical depth of the corona is varying independently of the luminosity (Haardt et al. 1997).

6. Summary

In this paper we present the *ROSAT* and *ASCA* observations obtained during the 1995 monitoring campaign of 3C 390.3. The results can be summarized as follows:

- We obtained the first well sampled X-ray light curve from an AGN on time scales of days to months. Large amplitude flaring was observed with variability time scale of about 12 days, and quiescent periods with markedly reduced variability were observed on time scales as long as 30 days. While the amplitude of variability is larger than previously observed during X-ray monitoring campaigns, this is probably due to the fact that this campaign was much longer. While the time scale of variability seems slower than in many other well studied X-ray variable AGN, this may be reconciled with the greater luminosity ($2 - 4 \times 10^{44} \text{ergs cm}^{-2} \text{s}^{-1}$).
- The HRI hardness ratio varies during the monitoring campaign, but this is likely due to the known time dependent gain change of the instrument and therefore cannot be used to investigate the spectral variability.
- The spectra from two *ASCA* observations made during the monitoring period can be fit with an absorbed power law and an iron $K\alpha$ line. No evidence for soft excess emission was found, indicating that the *ROSAT* HRI is sampling the X-ray power law. The absorption is significantly larger than the Galactic value and slightly larger than that found in a 1993 *ASCA* observation (Eracleous et al. 1996). The photon index from the brighter observation was significantly larger than that from the fainter observation, and a compilation of results from *ASCA* and *Ginga* observations indicate that the photon index is correlated with the flux on long time scales, a trend seen in several Seyfert 1 galaxies.

K.M.L. thanks Dan Harris and Andrea Prestwich for useful discussions regarding the *ROSAT* HRI calibration, and Tahir Yaqoob for a critical reading of the manuscript. K.M.L and R.E. acknowledge support through *ASCA* AO-3 Guest Observers program grant NAG 5-2547 and *ROSAT* AO-5 Guest Observers program grant NAG 5-2637. K.M.L. acknowledges support at RIKEN by a Science and Technology Agency fellowship.

Table 1. *ROSAT* HRI Observation Log and Fluxes

Sequence Number	Julian Date ¹ (2,440,000+)	Exposure ² (s)	Count Rate ³ (counts s ⁻¹)
rh701798	9719.694	2927	0.301 ± 0.011
rh701799	9722.684	2098	0.454 ± 0.016
rh701800	9725.538	1825	0.485 ± 0.017
rh701801	9728.656	1673	0.421 ± 0.017
rh701802	9731.576	1353	0.331 ± 0.017
rh701803	9734.561	1305	0.321 ± 0.017
rh701804	9737.546	1052	0.380 ± 0.020
rh701805	9740.597	1043	0.447 ± 0.021
rh701806	9744.312	712	0.384 ± 0.024
rh701807	9747.350	2941	0.349 ± 0.012
rh701808	9750.200	2999	0.436 ± 0.013
rh701809	9752.588	2521	0.424 ± 0.014
rh701810	9755.577	1588	0.362 ± 0.016
rh701811	9758.565	1253	0.354 ± 0.018
rh701812	9761.948	3159	0.394 ± 0.012
rh701813	9764.941	1788	0.353 ± 0.015
rh701814	9767.595	2190	0.321 ± 0.013
rh701815	9770.547	1259	0.336 ± 0.017
rh701816	9773.618	2315	0.340 ± 0.013
rh701817	9776.582	1268	0.321 ± 0.017
rh701818	9778.909	2045	0.333 ± 0.014
rh701819	9781.763	2618	0.374 ± 0.013
rh701820	9784.685	2578	0.457 ± 0.014
rh701821	9787.804	2219	0.588 ± 0.017
rh701822	9790.926	1311	0.778 ± 0.025
rh701823	9793.642	1834	0.964 ± 0.024
rh701824	9796.561	1794	0.844 ± 0.022
rh701825	9799.980	1997	0.685 ± 0.019
rh701826	9802.731	2287	0.544 ± 0.016
rh701827	9805.583	1473	0.547 ± 0.020
rh701796	9809.564	1316	0.560 ± 0.021
rh701795	9812.538	2922	0.558 ± 0.015
rh701794	9815.595	1896	0.530 ± 0.018
rh701793	9818.647	1592	0.514 ± 0.019
rh701730	9819.943	2430	0.534 ± 0.016
rh701731	9823.554	1641	0.567 ± 0.020
rh701732	9825.544	1551	0.497 ± 0.019
rh701733	9830.451	1460	0.529 ± 0.020
rh701734	9831.568	1800	0.484 ± 0.018
rh701735	9834.585	1483	0.452 ± 0.019
rh701737	9840.586	2815	0.548 ± 0.015

Table 1—Continued

Sequence Number	Julian Date ¹ (2,440,000+)	Exposure ² (s)	Count Rate ³ (counts s ⁻¹)
rh701738	9843.570	3048	0.594 ± 0.015
rh701739	9846.590	2224	0.530 ± 0.016
rh701740	9849.673	1531	0.483 ± 0.019
rh701742	9855.577	1906	0.428 ± 0.016
rh701743	9858.563	1586	0.488 ± 0.019
rh701744	9861.586	1394	0.596 ± 0.021
rh701745	9864.768	2030	0.557 ± 0.017
rh701746	9867.950	2120	0.604 ± 0.018
rh701747	9870.869	2119	0.602 ± 0.018
rh701748	9873.853	2037	0.530 ± 0.017
rh701749	9876.838	1717	0.507 ± 0.018
rh701750	9879.711	2457	0.536 ± 0.016
rh701751	9882.662	3209	0.446 ± 0.013
rh701752	9885.624	1168	0.425 ± 0.020
rh701753	9888.599	1910	0.414 ± 0.015
rh701754	9891.613	1663	0.489 ± 0.018
rh701755	9894.567	1687	0.397 ± 0.016
rh701757	9900.600	1401	0.266 ± 0.015
rh701758	9903.550	1883	0.255 ± 0.013
rh701759	9906.568	1891	0.289 ± 0.013
rh701760	9909.586	1538	0.300 ± 0.015
rh701761	9912.670	2675	0.308 ± 0.012
rh701762	9915.651	1805	0.316 ± 0.015
rh701763	9918.544	1187	0.333 ± 0.018
rh701764	9921.593	3089	0.354 ± 0.012
rh701765	9924.778	2137	0.352 ± 0.014
rh701766	9927.797	1639	0.321 ± 0.015
rh701767	9930.780	1804	0.391 ± 0.016
rh701768	9933.930	1629	0.399 ± 0.017
rh701769	9936.980	1562	0.511 ± 0.019
rh701770	9940.131	2318	0.507 ± 0.015
rh701772	9945.732	2051	0.633 ± 0.018
rh701773	9948.718	1885	0.624 ± 0.019
rh701774	9951.635	1975	0.660 ± 0.019
rh701775	9954.619	2065	0.791 ± 0.020
rh701776	9957.603	1943	0.894 ± 0.022
rh701777	9960.587	1805	0.855 ± 0.022
rh701778	9963.639	2550	0.733 ± 0.018
rh701779	9966.578	1595	0.664 ± 0.021
rh701780	9969.563	1925	0.704 ± 0.020
rh701781	9972.580	1847	0.967 ± 0.023

Table 1—Continued

Sequence Number	Julian Date ¹ (2,440,000+)	Exposure ² (s)	Count Rate ³ (counts s ⁻¹)
rh701782	9975.643	1956	0.862 ± 0.021
rh701783	9978.583	1689	0.731 ± 0.021
rh701784	9981.531	2585	0.688 ± 0.017
rh701785	9984.582	1336	0.558 ± 0.021
rh701786	9987.606	1847	0.571 ± 0.018
rh701787	9990.625	2527	0.636 ± 0.016
rh701788	9993.644	933	0.790 ± 0.030
rh701789	9996.761	1764	0.877 ± 0.023

Note. — Exposures and count rates have not been corrected for the off-axis response.

¹Observation time is given for midpoint of each observation; no barycentric correction has been performed.

²Exposure has been corrected for livetime.

³Using the distributed HRI response matrix and ignoring the effects of the gain change, 1 count/s corresponds to 2.93 and 3.04×10^{-11} ergs s⁻¹cm⁻² for photon indices 1.7 and 1.82 respectively and $N_H = 1.15 \times 10^{21}$ cm⁻².

Table 2. *ASCA* Observation Log

Detector	Exposure	Net Count Rate (counts s ⁻¹)
First Observation (TJD 9733.12) ^a		
SIS0	18204	0.604
SIS1 ^b	10844	0.509
GIS2	18122	0.356
GIS3	18122	0.432
Second Observation (TJD 9843.75) ^a		
SIS0	17298	1.080
SIS1	17300	0.899
GIS2	18760	0.600
GIS3	18770	0.702

^aJulian date of midpoint of the observation, 2,440,000+.

^bThe exposure time for this detector is lower, because only the data collected at high bit rate were used for spectral analysis; see text for details.

Table 3. *ASCA* Spectral Fitting Results

Parameter	First Observation	Second Observation
$N_H(\times 10^{22}\text{cm}^{-2})$		$0.115^{+0.012}_{-0.011}$
Photon Index	1.70 ± 0.03	1.82 ± 0.03
SIS0 PL norm ($\times 10^{-3}\text{photons keV}^{-1}\text{cm}^{-2}\text{s}^{-1}$)	4.39 ± 0.15	$8.18^{+0.26}_{-0.25}$
Iron Line Energy (keV)		$6.29^{+0.27}_{-0.28}$
Iron Line Width (keV)		0.34 (fixed)
Iron Line norm ($\times 10^{-5}\text{photons cm}^{-2}\text{s}^{-1}$)	$3.2^{+2.3}_{-2.4}$	$3.5^{+2.9}_{-2.6}$
Equivalent Width (eV)	167 ± 120	120^{+100}_{-90}
Observed Flux (2–10 keV; $\times 10^{-11}\text{ergs cm}^{-2}\text{s}^{-1}$)	1.8	2.8
Intrinsic Luminosity (2–10 keV; $\times 10^{44}\text{ergs s}^{-1}$)	2.6	4.0

Note. — The best fit $\chi^2 = 2165/2129$ d.o.f. All quoted errors are 90% confidence for two parameters of interest ($\Delta\chi^2 = 4.61$). The line width could not be constrained, so it was fixed at the best fit value during evaluation of errors of the other parameters.

Table 4. Photon Index History

Date	Instrument	2-10 keV Flux ($\times 10^{-11}\text{ergs cm}^{-2}\text{s}^{-1}$)	Photon Index	Reference
1988.86	<i>Ginga</i>	4.2	^a $1.89^{+0.03}_{-0.02}$	1
1991.12	<i>Ginga</i>	2.4	^a $1.71^{+0.11}_{-0.08}$	1
1993.88	<i>ASCA</i> SIS	1.75	^a $1.70^{+0.03}_{-0.02}$	2
1995.15	<i>ASCA</i> SIS+GIS	1.8	^b 1.72 ± 0.04	3
1995.125	<i>ASCA</i> SIS+GIS	2.8	^b 1.84 ± 0.03	3

References. — (1) Wozniak et al. 1996; (2) Eracleous et al. 1996; (3) this paper.

^aObtained from fits which use a reflection model (see text).

^bObtained from fitting spectra below 5 keV only (see text).

REFERENCES

- Alef, W., Wu, S. Y., Preuss, E., Kellerman, K. I., & Qiu, Y. H. 1996, *A&A*, 308, 376
- Barr, P., et al. 1980, *MNRAS*, 193, 549
- Clavel, J., & Wamsteker, W. 1987, *ApJ*, 329, 9
- David, L. P., Harnden, F. R., Kearns, K. E., & Zombeck, M. V. 1996, *The ROSAT High Resolution Imager (HRI) Calibration Report*
- Dietrich, M., et al. 1997, in preparation
- Edelson, R., et al. 1996, *ApJ*, 470, 364
- Eracleous, M. & Halpern, J. P. 1994, *ApJS*, 90, 1
- Eracleous, M., Halpern, J. P., & Livio, M. 1996, *ApJ*, 459, 89
- Haardt, F., Maraschi, L., & Ghisellini, G. 1997, *ApJ*, in press
- Inda, M., et al. 1994, *ApJ*, 420, 143
- Lawrence, A., & Papadakis, I. E., 1993 *ApJL*, 414, 85
- Leighly, K. M., Kunieda, H., Awaki, H., & Tsuruta, S. 1996, *ApJ*, 463, 158
- Leighly, K. M., & O’Brien, P. T. 1997, accepted for publication in *ApJL*
- Leighly, K. M., et al. 1997 in preparation
- Matt, G., Perola, G. C., Piro, L., & Stella, L. 1992, *A&A*, 257, 63
- Murphy, E. M., Lockman, F. J., Laor, A., & Elvis, M. 1996, *ApJS*, 105, 369
- Mushotzky, R. F., Baity, W. A., & Peterson, L. E. 1977, *ApJ*, 212, 22
- Nandra, K., Pounds, K. A., Stewart, G. C., George, I. M., & Hayashida, K. 1991, *MNRAS*, 248, 760
- Nandra, K., & Pounds, K. A. 1994, *MNRAS*, 268, 405
- O’Brien, P. T., et al. 1997, in preparation
- Reynolds, C. S., Fabian, A. C., Nandra, K., Inoue, H., Kunieda, H., & Iwasawa, K. 1995, *MNRAS*, 277, 901
- Veilleux, S. & Zheng, W. 1991, *ApJ*, 377, 89
- Weaver, K. A., Nousek, J., Yaqoob, T., Hayashida, K. & Murakami, S. 1995, *ApJ*, 451, 147
- Wozniak, P.R., Zdziarski A.A., Smith D., Madejski G.M. 1997, submitted to *MNRAS*
- Yaqoob, T., & Warwick, R. S. 1991, *MNRAS*, 248, 773
- Zdziarski, A. A., Johnson, W. N., Done, C., Smith, D., & McNaron-Brown, K. 1995, *ApJL*